Journal of Materials Chemistry

Cite this: *J. Mater. Chem.*, 2011, **21**, 6736

www.rsc.org/materials

PAPER

Surface induced negative photoconductivity in p-type ZnSe : Bi nanowires and their nano-optoelectronic applications

Xiwei Zhang, Jiansheng Jie,* Zhi Wang, Chunyan Wu, Li Wang, Qiang Peng, Yongqiang Yu, Peng Jiang and Chao Xie

Received 4th January 2011, Accepted 3rd March 2011
DOI: 10.1039/c1jm00035g

Single-crystal p-type ZnSe nanowires (NWs) with zinc blende structure and [21–1] growth direction were synthesized by using bismuth (Bi) as dopant *via* a thermal co-evaporation method. The ZnSe : Bi NWs showed evident p-type conductivity with hole concentration up to 4.1×10^{18} cm^{-3} after the acceptor activation. Negative photoconductivity was first investigated in the p-ZnSe NWs, *i.e.*, the conductivity of the NWs under light was dramatically lower than that in the dark. Surface effects arising from oxygen absorption and photo-desorption were suggested to be responsible for this. By using Al as the Schottky gate, high-performance nano-metal-semiconductor field-effect transistors (nanoMESFETs) were constructed, and measurements on the Al/p-ZnSe NW Schottky diode also revealed the bias-dependent photoresponse. It is expected that the p-type ZnSe : Bi NWs will have great potential in nano-optoelectronic applications.

1. Introduction

One of the most distinguishing features of nanostructures is the surface effect, which rises from their large surface-to-volume and plays an important role in dominating the electrical, mechanical, and chemical properties of the nanostructures.[1–5] For instance, the roughness at Si nanowires surfaces enhanced diffuse reflection or backscattering of phonons at interfaces, resulting in a remarkable increase in thermoelectric figures of merit.[1] P-type silicon nanowires (NWs) showed enhanced conductivity in air due to the surface absorption of moisture, and the large surface energy band bending even turned the n-type Si NWs to p-type.[2] Surface transfer doping is therefore becoming feasible *via* interface charge transfer instead of conventional doping by introducing foreign impurities.[3,4] On the other hand, photoconductivity in semiconductors is well recognized; the generation of photocurrent makes the semiconductors more conductive upon light illumination. However, Dai *et al.* found that the conductivity of single-wall carbon nanotubes (SWCNTs) decreased in light, namely negative photoconductivity, due to photoinduced molecular desorption from the nanotube surface,[5] but this phenomenon seems to be restricted to SWCNTs and has seldom been observed in other semiconductor nanostructures so far. Owing to the unique and fascinating properties originating from the surface effect, it has already been a critical issue to further exploit the surface effect in nanostructures and utilize it for diverse nanodevice applications in current nanoscience research.

As a wide direct band gap II–VI semiconductor, ZnSe (E_g = 2.7 eV) has great potential in optoelectronic devices, such as light emitting diodes (LED), green-blue laser diodes, and solar cells *etc.*[6–8] ZnSe nanostructures have attracted much attention and their synthesis and optical properties have been intensively studied.[9–11] Despite these progresses, the practical applications of ZnSe nanostructures are still hindered by the difficulty in controlling their transport properties, particularly p-type conductivity. It is known that the p-type doping in ZnSe films suffers from a serious self-compensation effect, that is, doping of the acceptors will inevitably introduce one or more donor defects, thus counteracting the effect of p-type doping. As for the ZnSe nanostructures, they are single crystal and grown by a catalyst method, thus avoiding the defects induced by lattice-mismatched substrates. Therefore, it is expected that more efficient p-type doping will hopefully be achieved in ZnSe nanostructures. Song *et al.* reported the synthesis of p-type ZnSe NWs by using As doping.[12] Nevertheless, p-type ZnSe nanostructures with non-toxic dopants need to be developed in further research.

Herein, we report the synthesis of p-type ZnSe NWs by using bismuth (Bi) as the acceptor dopant *via* a simple co-evaporation method. Nanodevices based on single ZnSe : Bi NWs were constructed to study their transport properties. Surface induced negative photoconductivity was first observed in the p-ZnSe NWs, which also led to a novel bias-dependent photoresponse of Al/p-ZnSe NW Schottky diodes. The successful fabrication of p-ZnSe NWs not only provides a new platform for studying the surface dominated optoelectronic properties of semiconductor

School of Electronic Science and Applied Physics, Hefei University of Technology, Hefei, Anhui, 230009, P. R. China. E-mail: jason.jsjie@gmail.com

nanostructures but also opens the opportunities for a host of new nano-optoelectronic devices.

2 Experimental details

ZnSe : Bi NWs were synthesized by using ZnSe powder (Aldrich, 99.99%) and bismuth powder (Aladdin, 99.99%) as the source material and the p-type dopant, respectively, in a horizontal alumina tube furnace. In a typical experiment, ZnSe powder (0.3 g) was first loaded into an alumina boat and transferred to the center region of the furnace. Another boat filled with 0.15 g Bi powder was then placed at the upstream position. Silicon substrates coated with 10 nm Au catalyst were placed at the down stream ~12 cm from the ZnSe source. The reaction chamber was flushed and filled with a gas mixture of 50 sccm Ar and H_2 (5% in volume) after it was evacuated to a base pressure of 6×10^{-3} Pa. The pressure in the tube was adjusted to 150 Torr before heating. The temperatures of the ZnSe powder, Bi powder and silicon substrates were maintained at 1000 °C, ~900 °C, and ~700 °C, respectively, during the experiment. After a growth duration of 1.5 h, the system was cooled down to room temperature and the Si substrates were taken out of the furnace. A layer of yellow wool-like product could be observed on the substrate surfaces.

Morphologies and structures of the as-synthesized ZnSe : Bi NWs were characterized by X-ray diffraction (XRD, Rigaku D/Max-rB), field-emission scanning electron microscopy (FESEM, SIRION 200 FEG) and high-resolution transmission electron microscopy (HRTEM, JEOL JEM-2010, at 200 kV). Compositions of the ZnSe : Bi NWs were analyzed by X-ray photoelectron spectroscopy (XPS, Thermo ESCALAB 250).

To assess the electrical and photoconductive properties of the ZnSe : Bi NWs, two types of field-effect transistors (FETs), including nano-metal-oxide-semiconductor FETs (nano-MOSFET) and nano-metal-semiconductor FETs (nano-MESFET), were constructed based on the individual ZnSe : Bi NWs. To fabricate the MOSFETs, the as-synthesized ZnSe NWs were first dispersed on a SiO_2 (300 nm)/p^+-Si substrate, and subsequently photolithography and lift-off processes were used to define the Ti(1 nm)/Au(50 nm) source and drain electrodes on the NWs. The degenerately doped Si substrate then acted as the global back gate. As for the nanoMESFETs, an aluminium top Schottky gate (50 nm) was fabricated by an additional photolithography process. All the electrical measurements were conducted at room temperature with a semiconductor characterization system (Keithley 4200-SCS). The white light from the optical microscopy on the probe station was used as the light source for detection of the photoconductive properties of the p-type ZnSe : Bi NWs.

3 Results and discussion

3.1 Characterization of p-type ZnSe : Bi NWs

Fig. 1a shows the typical FESEM image of the as-synthesized ZnSe : Bi NWs. It is seen that the NWs have a uniform geometry with diameter in the range of 100–700 nm and length of several tens of micrometres. The gold catalyst caps can be clearly observed at the tips of the NWs (inset in Fig. 1a and Fig. 1c), indicating that the NWs were grown *via* a conventional vapor-liquid-solid (VLS) process. In the XRD pattern of the ZnSe : Bi NWs (Fig. 1b), all the diffraction peaks can be assigned to zinc blende ZnSe (JCPDS No. 88-2345) and no impurity phases are detected, suggesting the high phase purity of the product. TEM investigations also confirm that the ZnSe : Bi NWs have single-crystal zinc blende structure with a growth orientation of [21–1] (Fig. 1c and d). XPS measurements were also performed to detect the compositions of the ZnSe : Bi NWs and two weak peaks corresponding to Bi 4f5/2 and Bi 4f7/2 core level emissions, respectively, can be observed near the Se 3p1/2 and Se 3p3/2 peaks (Fig. 1e), revealing the presence of trace Bi (~0.5 at.%) in the ZnSe NWs. Considering that the ZnSe NWs are uniform and clean with few impurities and particles, the Bi signal is most likely coming from the Bi atoms that were successfully incorporated into the ZnSe NWs.

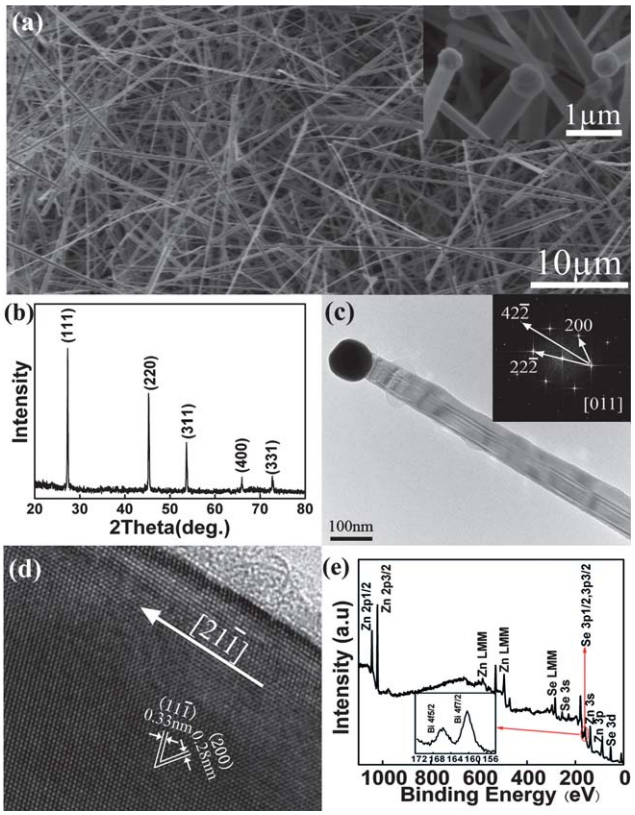

Fig. 1 (a) Typical FESEM images of the as-synthesized ZnSe : Bi NWs. (b) XRD pattern of the ZnSe : Bi NWs. (c) Low-resolution TEM image of a single ZnSe : Bi NW. Inset shows the corresponding SAED pattern. (d) HRTEM image of the ZnSe : Bi NW. (e) XPS survey spectrum of the ZnSe : Bi NWs. Inset shows two XPS peaks that originated from Bi in ZnSe NWs.

3.2 Electrical characterization and negative photoconductivity of p-ZnSe NWs

Fig. 2a depicts the typical source–drain current (I_{ds}) *versus* source–drain voltage (V_{ds}) curves measured from a single ZnSe : Bi NW. The as-synthesized ZnSe : Bi NWs are highly insulative with a conductivity as low as $\sim 2.9 \times 10^{-5}$ S cm^{-1}. In contrast, the NW conductivity has been dramatically improved to 4.1×10^{-4} S cm^{-1} and 0.59×10^{-2} S cm^{-1}, respectively, after

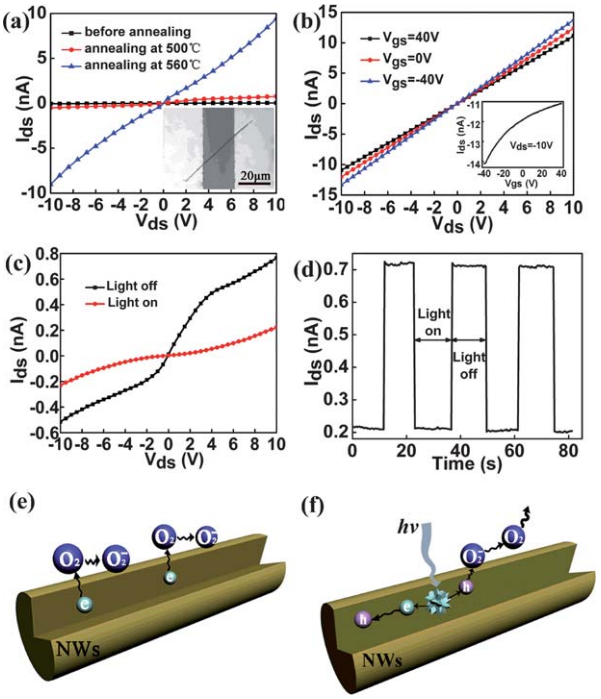

Fig. 2 (a) $I_{ds} - V_{ds}$ curves of the p-ZnSe NW before and after annealing. Inset shows the optical image of the device. (b) Electrical transport characteristics of the back-gate FET based on a single ZnSe : Bi NW. $I_{ds} - V_{ds}$ curves are measured at varied V_{gs} ranging from −40 V to 40 V in a step of 40 V. Inset shows the $I_{ds} - V_{gs}$ curve at $V_{ds} = -10$ V. (c) $I_{ds} - V_{ds}$ curves of the p-ZnSe NW measured in light and in dark, respectively. (d) Photoresponse of the p-ZnSe NW to pulsed light at $V_{ds} = 10$ V. Schematic illustrations of the (e) adsorption and (f) photodesorption of oxygen molecules.

a rapid thermal annealing (RTA) process in Ar atmosphere at 500 °C and 560 °C for 5 min. It is noted that identical results are obtained no matter whether the NWs were annealed before or after electrode fabrication, implying that the conductivity enhancement is not a result of the electrode/NW contact improvement but is due to the activation of Bi acceptors in the NWs under post-annealing, which is consistent with a previous study on As-doped ZnSe NWs.[12] Fig. 2b shows the gate-dependent $I_{ds} - V_{ds}$ curves measured at varied gate voltage (V_{gs}) from −40 V to 40 V for the nanoMOSFET. It is found that the device shows a pronounced p-type gating effect, *i.e.*, conductance of the ZnSe : Bi NW increases with the decreasing of V_{gs}, revealing the successful achievement of p-type conduction in ZnSe NWs *via* Bi doping. The field-effect hole mobility μ_h and carrier concentration n_h are deduced to be 0.91×10^{-2} cm^2 V^{-1} s^{-1} and 4.1×10^{18} cm^{-3}, respectively, from the transfer characteristics according to the following equations as:

$$\mu_h = \frac{dI_{ds}}{dV_{gs}} \frac{\ln(4h/d)L}{2\pi\varepsilon_0\varepsilon_{SiO_2}V_{ds}} \quad (1)$$

$$n_h = \sigma/\mu_h e \quad (2)$$

where the transconductance $g_m = dI_{ds}/dV_{gs}$ is extracted from the linear regime of the $I_{ds} - V_{gs}$ curve, ε_{SiO_2} is the dielectric constant of the gate SiO_2 (~3.9). L, h and d represent the NW channel length (20 μm), gate oxide layer thickness (300 nm), and the NW diameter (~200 nm), respectively. σ is the conductivity of the NWs after annealing at 560 °C. These results unambiguously demonstrate that an effective p-type doping has been achieved in the ZnSe NWs by using Bi as the dopant.

As a group V dopant, Bi appears to be a potential candidate for formation of defect complexes in the ZnSe NWs. First, Bi has a large ion radius of 1.63 Å (1.22 Å for Se), therefore it is a large-size-mismatched dopant for ZnSe, which may lead to the generation of nearby vacancies in the NWs. Secondly, Bi has a lower electronegativity (2.02 eV for Bi and 2.55 eV for Se), which makes it easier to occupy the Zn antisite instead of substituting the Se atom. We note that the peaks located at 157.0 eV and below 157.0 eV that correspond to isolated Bi and Bi–Zn bonding,[13] respectively, did not appear in the XPS spectrum, implying that the Bi_{Se} (Bi occupying Se site) and Bi_i (interstitial atom) defects are absent in the ZnSe : Bi NWs. On the other hand, the 160.05 eV peak could be assigned to Bi–Se bonding, verifying that most of the Bi that was incorporated into the ZnSe NWs should exist as Bi_{Zn} defects.[13] At the same time, Zn vacancies (V_{Zn}) will be induced by Bi dopant and eventually lead to the formation of Bi_{Zn}–$2V_{Zn}$ complexes, which have been demonstrated to be the most probable acceptor defects formed in ZnSe : Bi films due to their low formation energy and shallow acceptor level.[14,15] It is assumed that Bi atoms are incorporated into the as-synthesized ZnSe NWs partly as Bi–H pairs.[16] H compensation will reduce the hole concentration and result in the high resistivity of the as-synthesized NWs. After annealing at 560 °C, the hole concentration is increased *via* dissociation of Bi–H bonding and activation of Bi acceptors.[17]

ZnSe is a promising material for blue light detection due to its appropriate band-gap of ~2.7 eV. In this work, the photoconductive properties of the p-type ZnSe : Bi NWs were further investigated. Fig. 2c depicts the typical *I*–*V* curves of the p-ZnSe NW measured in the dark and under light illumination, respectively. Surprisingly, different from the positive photoconductivity (conductivity increases in light) for most of the semiconductors, evident negative photoconductivity has been observed for the p-ZnSe NWs, *i.e.*, the conductivity in light is much lower than that in the dark. From the time response of the p-ZnSe NW in Fig. 2d, a response ratio of I_{dark}/I_{light} of ~3.5 is revealed. The device also shows good stability and reproducibility as well as a fast response to the pulsed light with a rise and fall time ~0.38 s and ~0.4 s, respectively. Besides the ZnSe : Bi NWs, p-type ZnSe : N NRs also show the same negative photoconductivity, in contrast to positive photoconductivity for n-type ZnSe : Cl NWs (data not shown), implying that the negative photoconductivity is an inherent property of p-type ZnSe nanostructures.

It is known that the surface effect induced by oxygen adsorption and photo-desorption plays an important role in regulating the photoresponse of semiconductor nanostructures, such as SWCNTs, ZnO NWs, and CdS NRs.[5,18,19] The negative photoconductivity of the p-ZnSe NWs could be interpreted by this mechanism as well. Under ambient conditiond in the dark, oxygen molecules will be absorbed onto the surface of p-ZnSe NW and ionized by capturing electrons from the NW due to its strong electronegativity (Fig. 2e):

$$O_2(g) + e^- \rightarrow O_2^-(ad) \quad (3)$$

The transfer of electrons from the NW to oxygen molecules will result in an increase of the hole concentration in the p-ZnSe NWs, therefore a larger conductance in the dark is observed. When the light is turned on, electron-hole pairs are generated by the photons with energy higher than the band-gap of ZnSe:

$$hv \rightarrow e^- + h^+ \quad (4)$$

Owing to the up bending of the valance band by the surface potential, photo-generated holes tend to migrate to the NW surface and then discharge the adsorbed oxygen ions through a surface electron-hole recombination process as follows (Fig. 2f):

$$h^+ + O_2^-(ad) \rightarrow O_2(g) \quad (5)$$

At the same time, photo-generated electrons will recombine with the holes in the p-ZnSe NWs, leading to the decrease of the NW conductivity in the light. The current could recover after the light is turned off due to the reabsorption of the oxygen molecules in air.

3.3 NanoMESFETs based on single p-ZnSe NWs

NanoMESFETs are emerging as promising building blocks for future nano-optoelectronic applications due to the simple fabrication process and the capability to scale up.[20,21] With the successful realization of p-type doping, p-channel nanoMESFETs based on the p-ZnSe NWs are also studied in this work. Fig. 3a presents the schematic illustration of the nanoMESFET device, in which an aluminium Schottky gate was fabricated between two adjacent Au Ohmic contact electrodes. At first, the electrical characteristics of the Al/p-ZnSe NW Schottky contact are determined by applying a voltage bias between the Al gate and the Au electrode (Fig. 3b). It is noted that the diode shows excellent rectification behavior with a turn-on voltage of ~2.1 V, a low reverse current of $\sim 10^{-12}$ A, and a high rectification ratio larger than 10^3. The ideality factor (n) of the Schottky diode was deduced to be ~2.73 based on the equation:

$$n = \frac{q}{kT}\frac{dV}{d\ln I} \quad (6)$$

where q, k and T represent the electronic charge, Bolzmann's constant and absolute temperature, respectively. This value is larger than that for an ideal diode ($n = 1$). The deviation is likely caused by the enhanced tunneling current in a nanoscale Schottky contact.[22]

The high quality Schottky contact between the Al gate and the p-ZnSe NW allows the nanoMESFET to function with good performance. Fig. 3c depicts the $I_{ds} - V_{ds}$ curves measured at varied V_{gs}. During the measurements, the source electrode was grounded and the gate voltage was limited to within ±1 V to avoid excessive gate leakage. The measurements were performed in the dark. It is noted that I_{ds} increases monotonously with the decreasing of V_{gs} from 0.15 V to −0.9 V in a voltage step of −0.15 V, revealing that the device is a p-channel nanoMESFET. Moreover, the threshold voltage (V_{th}) is determined to be about −0.4 V by extrapolating the linear region of the $I_{ds} - V_{gs}$ curve (Fig. 3d), and the device is turned off at zero gate bias, indicating that the device is working at p-channel *E*-mode. A high on/off current ratio of $\sim 10^3$ is obtained from the logarithmic $I_{ds} - V_{gs}$ curve when V_{gs} changes from −0.9 V to 0.6 V. The gate leakage current (I_g) is at the same order of magnitude with the source–drain off-current but much lower than the source–drain on-current (Fig. 3d). A transconductance of ~3 nS is deduced from the linear regime of the $I_{ds} - V_{gs}$ curve. As compared with the back-gate nanoMOSFETs mentioned above, the nanoMESFET has exhibited much more excellent characteristics in terms of smaller operation voltage, higher transconductance, and larger on/off current ratio. The more effective channel modulation resulting from the good Al/p-ZnSe NW Schottky contact as well as the top surrounding Schottky gate configuration should be responsible for the substantial improvement of the device performance.[23]

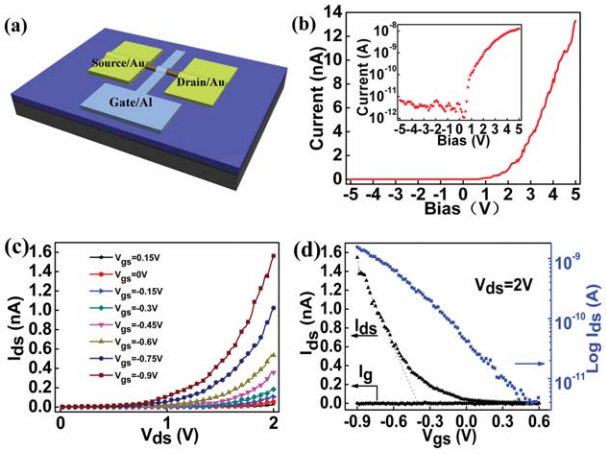

Fig. 3 (a) Schematic illustration of the *p*-channel nanoMESFET based on a single p-ZnSe NW. (b) $I - V$ characteristics of the Al/p-ZnSe NW Schottky contact. Inset shows the $I - V$ curve on a logarithmic scale. (c) $I_{ds} - V_{ds}$ curves measured at varied V_{gs} ranging from 0.15 V to −0.9 V in a step of −0.15 V. (d) $I_{ds} - V_{gs}$ and $I_g - V_{gs}$ curves measured at $V_{ds} = 2$ V.

3.4 Photoresponse of Schottky diodes based on p-ZnSe NWs

Owing to the small sizes and the capabilities for localized/polarized detection, Schottky diodes formed by metal/semiconductor nanostructure junctions have potential applications as high-performance photodetectors.[24–26] Fig. 4 shows the photoresponse of the Al/p-ZnSe NW Schottky diode to incident light. Interestingly, the nano-Schottky diode exhibits quite different device characteristics from the conventional Schottky photodetector. That is, both negative photoresponse and positive photoresponse have occured in one device. The former is observed when the diode is forward biased, whereas the latter shows when the device is reversely biased. At forward bias, I_{light} is smaller than I_{dark} but still in the same order of magnitude (Fig. 4a). At reverse bias, however, I_{light} is about two orders of magnitude larger than I_{dark} and the device shows fast response to the pulsed incident light (Fig. 4b). To the best of our knowledge, these novel phenomena have been first observed in the Schottky

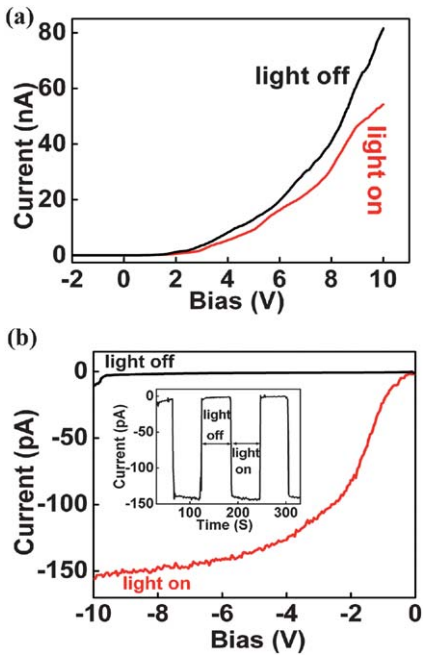

Fig. 4 Photoresponse of the Al/p-ZnSe Schottky diode at (a) forward bias. (b) reverse bias. Inset in (b) shows the time response of the diode at a reverse bias of −10 V.

photodiodes and have not been observed in film/bulk devices or other nanodevices yet.

To interpret the distinct photoresponse characteristics of the Al/ZnSe : Bi NW diode, the energy band diagrams of the diode are illustrated in Fig. 5. When no bias is applied, the band of the p-ZnSe NW near the metal/semiconductor interface is bended downwards and the holes are depleted in the near-surface area of the NW. At the forward bias, the Fermi level of p-ZnSe NW moves down, allowing the holes in the NW pass through the Schottky barrier and reach the electrode. That means the diode is turned on. When the light is turned on, the whole part of the NW can absorb the light, leading to the generation of electron-hole pairs, which will then be separated by the electric filed between the Au and Al electrodes and forming the photocurrent. In this case, the device functions the same as that without Schottky contact. According to the mechanism described above, it is reasonable that the device shows negative photoresponse at forward bias. In contrast, when the diode is reversely biased, the energy band of p-ZnSe NW will bend downwards and a larger space-charge region is formed. The electric field in the space-charge region has the direction from metal (Al) to the semiconductor (p-ZnSe NW). Due to the large Schottky barrier at the interface, holes can hardly drift from the Al electrode into the NW, resulting in a low dark current. When upon light illumination, electron-hole pairs generated by the absorbed photons in the space-charge region are separated by the electric field in opposite directions, constituting the photocurrent. The photo-generated electrons are injected into the Al electrode and the photo-generated holes are diffused into the inside part of the semiconductor. When the light is turned off, the photo-generated electron-hole pairs disappear and the current decreases again. Since the photocurrent is governed by the metal/semiconductor junction, the surface effect will not significantly affect the photocurrent anymore. As a result, a positive photoresponse is observed for the Al/p-ZnSe NW diode at reverse bias.

4 Conclusion

In conclusion, Bi-doped p-type ZnSe NWs were successfully synthesized by using bismuth as the dopant *via* an *in situ* doping process. The ZnSe : Bi NWs have zinc blende single-crystal structure with growth orientation of [21–1]. P-type conduction of the ZnSe NWs is attributed to the formation of Bi_{Zn}–$2V_{Zn}$ complexes with the incorporation of Bi. In addition, a post-annealing process is necessary to activate the acceptors in NWs. A negative photoresponse is observed for the p-ZnSe NW due to the surface effects resulting from absorption and photo-desorption of oxygen molecules in the air. P-channel E-mode nano-MESFETs were successfully constructed based on the p-ZnSe NWs by using Al as the top surrounding Schottky gate. The devices show a threshold voltage of about −0.4 V, trans-conductance of about 3 nS, and on/off current ratio of $>10^3$, which have been greatly improved compared to that of the back-gate nanoMOSFETs. Moreover, a bias-dependent photo-response is observed in Al/p-ZnSe NW Schottky diodes, which have negative photoresponse at forward bias, while positive photoresponse at reverse bias. Our results demonstrate that the surface effects of the nanostructures can dominate their optoelectronic properties. On the other hand, nanodevices with novel device functions could be constructed if utilizing the surface effects appropriately. These nanodevices could be used as important building blocks for next-generation nano-optoelectronics.

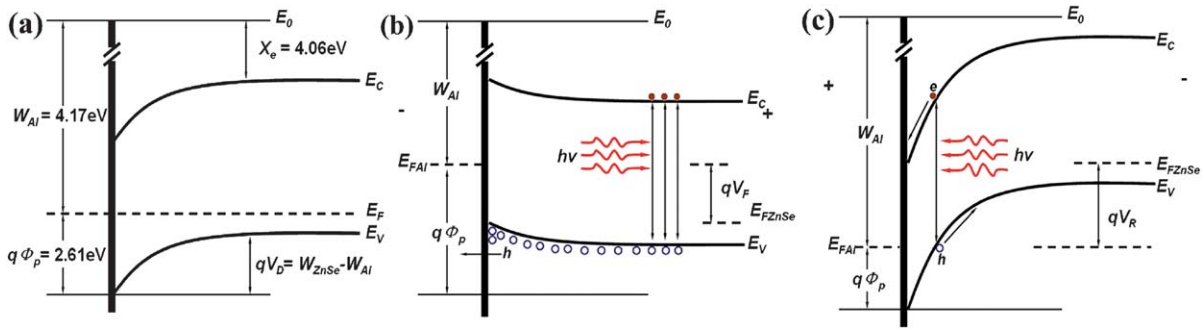

Fig. 5 Energy band diagrams of the Al/p-ZnSe Schottky diode at (a) zero bias. (b) forward bias. (c) reverse bias.

Acknowledgements

This work was supported by the National Natural Science Foundation of China (NSFC, Nos. 60806028 and 20901021), Program for New Century Excellent Talents in Universities of the Chinese Ministry of Education (No. NCET-08-0764), the Major Research plan of the National Natural Science Foundation of China (No. 91027021), and the Fundamental Research Funds for the Central Universities.

References

1 A. I. Hochbaum, R. Chen, R. D. Delgado, W. J. Liang, E. C. Garnett, M. Najarian, A. Majumdar and P. D. Yang, *Nature*, 2008, **451**, 163.
2 J. S. Jie, W. J. Zhang, K. Q. Peng, G. D. Yuan, C. S. Lee and S. T. Lee, *Adv. Funct. Mater.*, 2008, **18**, 3251.
3 G. D. Yuan, T. W. Ng, Y. B. Zhou, F. Wang, W. J. Zhang, Y. B. Tang, H. B. Wang, L. B. Luo, P. F. Wang, I. Bello, C. S. Lee and S. T. Lee, *Appl. Phys. Lett.*, 2010, **97**, 153126.
4 C. S. Guo, L. B. Luo, G. D. Yuan, X. B. Yang, R. Q. Zhang, W. J. Zhang and S. T. Lee, *Angew. Chem., Int. Ed.*, 2009, **48**, 9896.
5 R. J. Chen, N. R. Franklin, J. Kong, J. Cao, T. W. Tombler, Y. G. Zhang and H. J. Dai, *Appl. Phys. Lett.*, 2001, **79**, 2258.
6 J. Ren, K. A. Bowers, B. Sneed, D. L. Dreifus, J. W. Cook and J. F. Schetzina, *Appl. Phys. Lett.*, 1990, **57**, 1901.
7 M. A. Haase, J. Qiu, J. M. DePuydt and H. Cheng, *Appl. Phys. Lett.*, 1991, **59**, 1272.
8 P. Mahawela, G. Sivaraman, S. Jeedigunta, J. Gaduputi, M. Ramalingam and S. Subramanian, *Mater. Sci. Eng., B*, 2005, **116**, 283.
9 X. T. Zhang, Z. Liu, Y. P. Leung, Q. Li and S. K. Hark, *Appl. Phys. Lett.*, 2003, **83**, 5533.
10 S. L. Xiong, B. J. Xi, C. M. Wang, G. C. Xi, X. Y. Liu and Y. T. Qian, *Chem.–Eur. J.*, 2007, **13**, 7926.
11 Y. P. Leung, Choy, C. H. Wallace, I. Markov, G. K. H. Pang, H. C. Ong and T. I. Yuk, *Appl. Phys. Lett.*, 2006, **88**, 183110.
12 H. S. Song, W. J. Zhang, G. D. Yuan, Z. B. He, W. F. Zhang, Y. B. Tang, L. B. Luo, C. S. Lee, I. Bello and S. T. Lee, *Appl. Phys. Lett.*, 2009, **95**, 033117.
13 Y. Q. Shen, N. Xu, W. Hu, X. F. Xu, J. Sun, Z. F. Ying and J. D. Wu, *Solid-State Electron.*, 2008, **52**, 1833.
14 S. Limpijumnong, S. B. Zhang, S. H. Wei and C. H. Park, *Phys. Rev. Lett.*, 2004, **92**, 155504.
15 U. Wahl, E. Rita, J. G. Correia, A. C. Marques, E. Alves and J. C. Soares, *Phys. Rev. Lett.*, 2005, **95**, 215503.
16 T. Miki, J. F. Wang, A. Omino and M. Isshiki, *J. Cryst. Growth*, 1999, **200**, 399.
17 D. J. Chadi, *Phys. Rev. B: Condens. Matter*, 1999, **59**, 15181.
18 R. J. Chen, N. R. Franklin, J. Kong, J. Cao, T. W. Tombler, Y. G. Zhang and H. J. Dai, *Appl. Phys. Lett.*, 2001, **79**, 2258.
19 H. Kind, H. Q. Yan, B. Messer, M. Law and P. D. Yang, *Adv. Mater.*, 2002, **14**, 158.
20 R. M. Ma, L. Dai and G. G. Qin, *Nano Lett.*, 2007, **7**, 3300.
21 W. I. Park, J. S. Kim, G. C. Yi and H. J. Lee, *Adv. Mater.*, 2005, **17**, 1393.
22 G. D. J. Smit, S. Rogge and T. M. Klapwijk, *Appl. Phys. Lett.*, 2002, **81**, 3852.
23 P. T. Blanchard, K. A. Bertness, T. E. Harvey, L. M. Mansfield, A. W. Sanders and N. A. Sanford, *IEEE Trans. Nanotechnol.*, 2008, **7**, 760.
24 Y. F. Hu, J. Zhou, P. H. Yeh, Z. Li, T. Y. Wei and Z. L. Wang, *Adv. Mater.*, 2010, **22**, 3327.
25 N. S. Liu, G. J. Fang, W. Zeng, H. Zhou, F. Cheng, Q. Zheng, L. Y. Yuan, X. Zou and X. Z. Zhao, *ACS Appl. Mater. Interfaces*, 2010, **2**, 1973.
26 J. Zhou, Y. D. Gu, Y. F. Hu, W. J. Mai, P. H. Yeh, G. Bao, A. K. Sood, D. L. Polla and Z. L. Wang, *Appl. Phys. Lett.*, 2009, **94**, 191103.